New Magnetohydrodynamic (MHD) Lift Concept for More Efficient Missions to Mars and Neptune

Robert W. Moses[1], F. McNeil Cheatwood[2], and Christopher O. Johnston[3]
NASA Langley Research Center, Hampton, VA, 23681, United States

Sergey O. Macheret[4]
Purdue University, 701 W. Stadium Ave., West Lafayette, IN 47907-2045, United States

Bernard Parent[5]
University of Arizona, Tucson, AZ 85721, United States

Justin Little[6]
University of Washington, Seattle, WA, 98195, United States

Matthew Austin[7] and Andrew Aldrin[8]
Florida Institute of Technology, Melbourne, FL 32901, United States

Justin S. Green[9] and R. Anthony Williams[10]
NASA Langley Research Center, Hampton, VA, 23681, United States

The potential for using an applied magnetic field to augment the aerodynamic lift and drag of a hypersonic vehicle entering Neptune or Mars was studied. The study was conducted to assess whether magnetohydrodynamics (MHD) could boost aerodynamic lift and/or drag for aerocapture of a spacecraft into planetary orbit. MHD seemed well suited to create Lorentz forces during aerocapture when the flow is most ionized and conductive. Neptune and Mars were selected since larger payloads and faster trip times to each planet may substantially increase scientific and exploration opportunities. The results of the systems analysis presented herein suggest that a single MHD effector located off-centerline creates steering forces equaling whole-body aerodynamic forces and suggests a ground-breaking opportunity for new mission classes. The magnetic field required to produce these large forces is around 1 Tesla (T) having a mass roughly the same amount as the ballast used for recent Mars lander missions.

I. Nomenclature

A	=	Area
$\vec{B}$	=	magnetic field
Bx	=	magnetic field in the *x* direction (see Figure 1)
Bz	=	magnetic field in the *z* direction (see Figure 1)

[1] Aerospace Technologist, Atmospheric Flight and Entry Systems, AIAA Associate Fellow.
[2] Senior Technologist for Planetary Entry, Descent, and Landing; Atmospheric Flight and Entry Systems; AIAA Associate Fellow
[3] Aerospace Engineer, Aerothermodynamics Branch, AIAA Associate Fellow
[4] Professor, School of Aeronautics and Astronautics, AIAA Associate Fellow
[5] Associate Professor, Aerospace and Mechanical Engineering, AIAA Member
[6] Assistant Professor, William E. Boeing Department of Aeronautics & Astronautics, AIAA Member
[7] PhD Candidate
[8] Professor
[9] Aerospace Technologist, Atmospheric Flight and Entry Systems
[10] Aerospace Technologist, Atmospheric Flight and Entry Systems

CFD = computational fluid dynamics
CFDWARP = Combined CFD, MHD, and plasma sheath solver anchored at the University of Arizona
CD = Drag Coefficient
D = drag (when a force)
D = distance between electrodes (when volumetric analysis by CFDWARP)
$\vec{E}$ = induced electric field
e = electron charge
EDL = entry, descent, and landing
emf = Faraday electromotive force
$\vec{E} \times \vec{B}$ = drift motion along the flow of electrons and ions with respect to the bulk flow (slip effects)
$\vec{F}$ = Lorentz Force
Fx = *X* component of the resultant Lorentz force acting on the vehicle (see Figure 1)
Fy = *Y* component of the resultant Lorentz force acting on the vehicle (see Figure 1)
Fz = *X* component of the resultant Lorentz force acting on the vehicle (see Figure 1)
HARA = Hypersonic Aerothermodynamic Radiation Algorithm
K = load factor
L = lift
L/D = lift to drag ratio
LAURA = Langley Aerothermodynamic Upwind Relaxation Algorithm
M = ion mass
m = electron mass
MHD = magnetohydrodynamic
n_e = electron number density
n = number density of gas
POST2 = Program to Optimize Simulated Trajectories II
q = charge
T_e = electron temperature
$\vec{u}$ = local velocity
ν = ion-neutral collision frequency
ν_{ei} = rate of collisions with ions
ν_{en} = rate of collision with neutrals
σ = electrical conductivity (Siemens/meter)
$\vec{V}$ = velocity of the charge carriers (ions and electrons)
σ_{eff} = reduction in the effective conductivity due to slip effects
$\tilde{\sigma}$ = conductivity corrected for ion slip
$\widetilde{\Omega}$ = Hall parameter corrected for ion slip
Ω_e = electron Hall parameter
Ω_i = ion Hall parameter

II. Introduction

A new approach to generate drag and lift during atmospheric entry was analyzed during a recent NASA Innovative Advanced Concepts (NIAC) Phase 1 study.[1] The approach uses the principles of MHD to produce Lorentz forces that augment the aerodynamic lift and drag on the entry vehicle during atmospheric flight to achieve orbit capture or to land. See Fig. 1. The ionized flow becomes conductive at certain entry conditions allowing for a current flux (J) established by the placement of the electrode pair. This allows the harvesting of electricity. In the presence of a magnetic field (B), the conductive flow creates a force (F). Some forces (F) constitute lift (L) and drag (D) components (with respect to the spacecraft velocity vector).

This Phase 1 activity builds upon studies and ground-based subscale ionization experiments in regenerative aerobraking [2, 3], energy harvesting [4-8], MHD drag modulation [9-14] and heat flux mitigation [15, 16, 11]. For some hypersonic entries at Mars, strong Lorentz forces can be produced using magnetic field strengths between 1-2 tesla (T) that approach or exceed drag forces achievable by aerodynamic forces [9, 8]. Similar results have been illustrated for some Earth reentries [11]. A key difference of the proposed novel approach is positioning discrete magnets circumferentially around the forebody (see Figure 1) to create multiple asymmetric Lorentz forces that may be commanded independently to modulate lift and drag for controlling the entry vehicle while flying its tight entry

corridors at Neptune and Mars. Since electrical power can be generated from the ionized flow, the design offers an option to use electromagnets that are self-powered during the entry rather than using permanent magnets. Another advantage of the presence of strong magnetic fields is in attenuating the turbulence intensity of the boundary layer [15] when the electrical conductivity is high. Preliminary estimates show that the heat transfer to the surface could be reduced significantly when the gas temperature exceeds 7000 K and the magnetic field is greater than 1 T, as in these energetic entries. Convective heat flux reduction due to magnetic interaction with an ionized high enthalpy flow field has also been observed experimentally [16]. Such an effect has the potential to significantly decrease the mass of the ablative material.

To demonstrate the feasibility of using an applied magnetic field to generate lift and drag in an ionized hypersonic flow, this paper presents a computational analysis of potential Neptune and Mars entry scenarios. The Langley Aerothermodynamic Upwind Relaxation Algorithm (LAURA) Navier-Stokes solver [17] provided the hypersonic flowfield, while the CFDWARP code [18] provided the solution to Maxwell's equations at various MHD patch locations on the vehicle. The resulting Lorentz forces provide an MHD-derived lift and drag contribution, which may be controlled based on the MHD patch location and orientation. The basic MHD theory for this analysis is presented in Section III, while Section IV presents the computational approach. Section V and VI then present the results for the Neptune and Mars entry cases, respectively. Finally, Section VII proposes future work.

Potential destinations of interest include Neptune, Mars, Titan, and Earth return. Detailed analysis is presented herein for Neptune and Mars to illustrate the potential of this magnetohydrodynamics (MHD) approach to enable faster and larger payloads to be placed in orbit by substantially increasing the lift and/or drag force that are possible by aerodynamic approaches. Neptune and Mars were selected since larger payloads and faster trip times to each planet may substantially increase scientific and exploration opportunities. Entry conditions for Neptune and Mars were selected based on previous aerocapture studies for those two destinations.

For Neptune applications, the mid L/D concept developed for the 2004 study has been the baseline shape of the past. [19, 20] The tight entry corridor at Neptune required an aeroshell shape capable of L/D ratios around 0.8. [19, 20] Blunt body aeroshells generally provide a L/D ratio of around 0.2. Hence, that 2004 study selected a Mid L/D shape capable of achieving the higher L/D ratio. But, for Mars applications, previous architecture studies used blunt bodies such as the Hypersonic Inflatable Atmospheric Decelerator (HIAD). [21] Several recent studies on fast transits to Mars influenced the selection of the entry conditions considered during this study. [22-24]

Our analysis of the Neptune case eventually led to consideration of a blunt body shape as well for Neptune. The desired orientation of the Lorentz Force and physical constraints on magnet placement for orienting the B-field to create a side or lift force, with respect to the spacecraft velocity vector, led to this final aeroshell geometry selection.

Since the flow is conductive, electrical power can be harvested for powering the electromagnetic without requiring a power supply be brought from Earth. Initial estimates of the electromagnet system necessary to produce 1 T are shown herein.

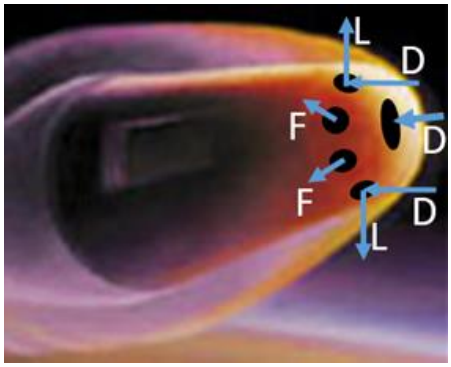

Fig. 1: Initial concept for independently commanded electromagnets to modulate lift and drag, where the MHD-derived Lorentz force (*F*) creates lift (*L*) and drag (*D*) components.

III. MHD Theory for EDL Applications

This section presents the basic characteristics of a hypersonic flow with an applied magnetic field. Later sections will present the results of the CFDWARP simulations, which implement these concepts. Subsection A presents an overview of the Lorentz force, which provides the dominant MHD impact. Subsections B and C then discuss the impact of Hall and ion slip effects, which may become large at certain conditions.

A. Impact of the Lorentz Force

The principles of MHD stem from the theory of electrical currents flowing in the presence of a magnetic field. Typical hypersonic flowfield simulations assume a quasi-neutral plasma and no induced or externally applied magnetic field. When a magnetic field (B) is applied to the hypersonic flowfield (u) through a magnet on the vehicle, the charged particles (q) experience the following Lorentz force (F):

$$\vec{F} = q\vec{u} \times \vec{B} \tag{1}$$

Since the charges of electrons and ions are of opposite signs, the electrons and ions are pulled apart, which creates a Faraday electromotive force (emf). The impact of this emf is captured in the generalized Ohm's Law, which is written as:

$$\vec{J} = \sigma\left(\vec{E} + \vec{V} \times \vec{B}\right) \tag{2}$$

where the Lorentz force term is the last term on the right, σ is the electrical conductivity, $\vec{J}$ is the current density, $\vec{E}$ is the electric field, and $\vec{V}$ is the velocity of the charge carriers. Note that Hall and ion slip effects are disregarded in Equation (2). Those effects (see subsection B below) would alter the generalized Ohm's law. For the configuration presented in Fig. 2, Equation (2) simplifies to the following.

$$J_y = (1 - K)\sigma u B_z \tag{3}$$

where K is the load factor (load resistance vs plasma resistance). In this case, the current that flows between the short-circuited electrodes is proportional to the conductivity of the plasma. This pair of electrodes is placed on the outer surface of the spacecraft. Hence, the conductivity of the flow is critical to the generation of large amounts of current within the plasma within MHD devices using during atmospheric entries.

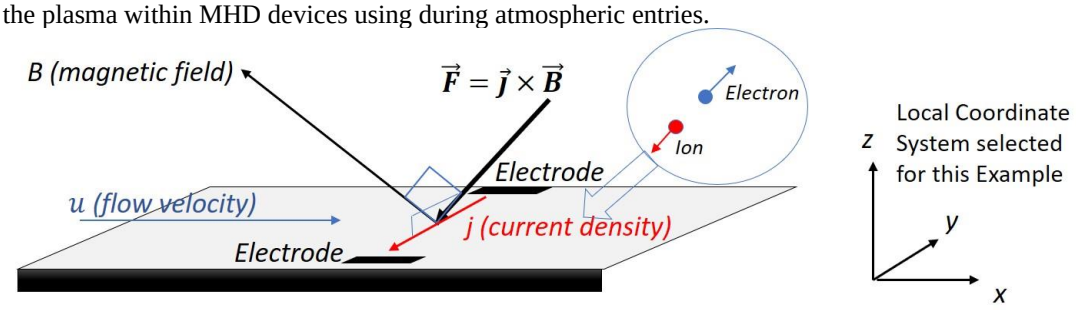

Fig. 2: Schematic of the Lorentz force creation for a magnetic field applied to a hypersonic flow. Current density (J) occurs between the two electrodes. Magnetic field (B) is shown as occurring in the x-z plane. The Resulting Lorentz Force (F) is Determined by Equation 4 and would be perpendicular to both J and B.

Generating a large amount of current is in turn critical for creation of large MHD-induced forces because the Lorentz force per unit volume corresponds to the cross product between the current density and the magnetic field vectors:

$$\vec{F} = \vec{J} \times \vec{B} \tag{4}$$

If $\vec{B}$ is inclined in the x-z plane and with respect to the surface for the example shown in Fig. 2 and has no y-component, and the flow velocity is along x axis, then the force per unit volume would have both axial (drag) and normal (lift) components, with no component along y axis:

$$F_x = -(1 - K)\sigma u {B_z}^2 \tag{5}$$

$$F_z = (1 - K)\sigma u B_z B_x \tag{6}$$

The scalar electrical conductivity is proportional to the number density n_e of principal charge carriers (electrons) and inversely proportional to the rate, or frequency, of their collisions with ions (ν_{ei}) and neutral molecules (ν_{en}):

$$\sigma = \frac{e^2 n_e}{m(\nu_{ei} + \nu_{en})} \tag{7}$$

Here, e and m are the electron charge and mass, respectively.

At low ionization fraction, $\frac{n_e}{n} \leq 10^{-3} - 10^{-2}$ (n is the number density of gas), electrons collide mostly with neutral molecules, and the conductivity is proportional to the ionization fraction [5]:

$$\sigma \approx 3 \times 10^5 \frac{n_e}{n} S/m \tag{8}$$

In this regime, the conductivity in hypersonic shock and boundary layers reaches ~10-500 S/m (Siemens per meter).

At high ionization fraction, $\frac{n_e}{n} \geq 10^{-3} - 10^{-2}$, electrons collide mostly with ions, and the conductivity does not depend on the ionization fraction, instead being determined by the electron temperature [5]:

$$\sigma \approx const \times {T_e}^{3/2} \tag{9}$$

In this regime, the conductivity reaches ~1000-3000 S/m. Because a high conductivity is critical to obtain large MHD forces, the MHD patch should be placed at a location on the spacecraft surface where the flow has a high conductivity. For typical re-entry flowfields, the temperature is high enough to lead to an ionization fraction above 0.1% and, therefore, the flow regions with the highest conductivity will be those where the electron temperature is the highest.

B. Hall and Ion Slip Effects

MHD forces not only increase with the magnitude of the flow velocity, plasma conductivity, and magnetic field strength, but are also sensitive to how the current flows in relation with the magnetic field and gas velocity vectors. Further, for maximum MHD forces, the current vector, flow velocity vector, and magnetic field vector should lie perpendicular to each other. As the magnetic field increases to very high values, two physical phenomena appear that lead to an attenuation of the Lorentz forces.

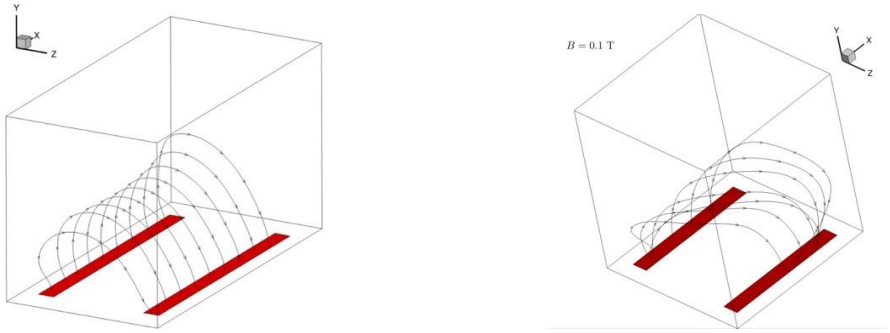

(a) Streamlines remain parallel (b) Streamlines distorted by Hall effects

Fig. 3: Example of current density streamlines that demonstrate Hall and ion slip effects. Red stripes are the electrodes shown in Fig. 2. Lines shown between each electrode pair (stripes) are the current density streamlines.

The first is the Hall effect. The Hall effect becomes important when the electron Hall parameter, defined as the ratio of the electron cyclotron frequency to the collision frequency, approaches or exceeds 1. When this occurs, the electrons and ions have a drift motion along the flow proportional to $\vec{E} \times \vec{B}$. This leads to the current not flowing perpendicular to the flow velocity, and thus reduces the Lorentz force because the latter is largest when the current and magnetic field vectors are perpendicular to each other.

The second is the ion slip effect. For larger values of the Hall parameter well in excess of one, the motion of electrons and ions is reduced so much that the ion-electron fluid starts to slip against the bulk neutral gas, i.e. moves at a velocity lower than that of bulk neutral gas, and the lower ion-electron velocity reduces the MHD effects (including body forces). This phenomenon is commonly referred to as the ion slip effect. The Hall and ion slip effects result in modification of the generalized Ohm's law (2). This can be shown to be equivalent to a reduction in the effective conductivity of the plasma as follows:

$$\sigma_{eff} = \frac{\tilde{\sigma}}{1+\widetilde{\Omega}^2} \tag{10}$$

Here the conductivity $\tilde{\sigma}$ and the Hall parameter $\widetilde{\Omega}$ corrected for ion slip are:

$$\tilde{\sigma} = \frac{\sigma}{1+\Omega_e\Omega_i} \tag{11}$$

$$\widetilde{\Omega} = \frac{\Omega_e}{1+\Omega_e\Omega_i} \tag{12}$$

Here σ is the scalar conductivity (see Equations (7)-(9)), and the electron (Ω_e)and ion (Ω_i) Hall parameters are, respectively:

$$\Omega_e = \frac{eB}{m(\nu_{ei}+\nu_{en})} \tag{13}$$

$$\Omega_i = \frac{eB}{M\nu_{in}} \tag{14}$$

where M and ν_{in} are the ion mass and ion-neutral collision frequency, respectively. Both the Hall and ion slip effects become dominant when the Hall parameter is high (higher than 10). Because the Hall parameter corresponds to the

product of the electron mobility and the magnetic field, and because the electron mobility is inversely proportional to the density of the gas mixture, it follows that Hall and ion slip effect occur when the magnetic field is very high and/or when the gas density is low. However, these effects can be exploited for modulating axisymmetric forces and moments, as will be illustrated later in a Mars entry case.

An example of the impact of Hall or ion slip effects on current streamlines is presented in Fig. 3. When the Hall effect is negligible, the current flows from one electrode to the other more or less perpendicular to the magnetic field and flow velocity (see Fig. 3a). But when the Hall effect is strong (Hall parameter higher than 1), a significant proportion of the current vector is parallel with the flow velocity.

IV. Analysis Overview

The present analysis is based on two steps. The first step is to obtain the conventional CFD solution using the LAURA Navier-Stokes solver coupled to the Hypersonic Aerothermodynamic Radiation Algorithm (HARA) radiation code. LAURA is a structured, multiblock, computational aerothermodynamic simulation code. [25] HARA is used to evaluate the shock-layer radiation that provides the radiative source term for the flowfield energy equations, which impacts the flowfield temperatures and chemistry [25]. The coupled LAURA/HARA simulations assume a quasi-neutral plasma and two-temperature thermochemical nonequilibrium. These simulations also assume a fully catalytic wall in radiative equilibrium. The solution and grid convergence criteria applied were consistent with the state-of-the-art applied for NASA flight programs. The finite-rate chemical kinetics models used will be given with each of the cases presented in Sections V and VI. These LAURA/HARA solutions provide the conventional aerodynamic lift and drag forces for each case, as well as the baseline flowfield properties for the second step of the analysis.

The second step of the analysis involves applying the CFDWARP code to a small patch of the LAURA flowfield. The MHD solver within CFDWARP obtains the current flowing between the short-circuited electrodes according to the generalized Ohm's law outlined in [26]. Such includes the Hall and ion slip effects for each ion (see [26] for details). This CFDWARP analysis holds the LAURA computed temperatures, velocity components, and number densities as fixed values, which are specified within CFDWARP using splines. With this LAURA flowfield as an input and a specified magnetic field, CFDWARP computes the resulting Lorenz forces, which are the MHD-derived lift and drag, defined by Equations (4) – (6), as well as the current path between the electrodes, defined by Equations. (2) - (3). These electrodes are used to harvest the electrical power required to power the electromagnet, which produces the applied magnetic field. Figure 4 shows an example of the flowfield patch considered by CFDWARP.

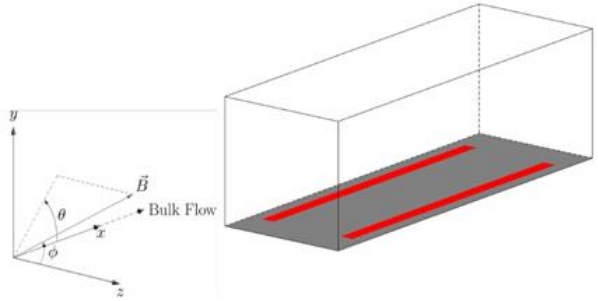

Fig. 4: Computational domain of the MHD patch simulation and definition of magnetic field orientation; the red strips are where the electrodes are located; the dark gray area is the surface of the spacecraft

Each of the patches considered by the CFDWARP analysis are located on the vehicle where the electromagnets are to be placed. As defined in Fig. 4, the electrodes are aligned so that the bulk flow from the LAURA solution occurs along the x-axis. The magnetic ($\vec{B}$) field can be oriented and modulated to create the Lorentz forces in the drag (-*x*), lift (*y*), and rolling moment (*z*) directions. It should be noted that the location of the patch and cone angle will dictate whether Lorentz forces along the x-axis produce drag or lift or both. The same is true for the creation of rolling moments or pitching moments. As defined in Fig. 3, the magnetic field components are defined as follows:

$$B_x = |B| cos\theta sin\phi \tag{15a}$$

$$B_y = |B| sin\theta sin\phi \tag{15b}$$

$$B_z = |B| cos\phi \tag{15c}$$

For all cases considered in this paper, the magnetic field strength, $|B|$, is fixed at 1.0 T. The length of computational domain is 0.2 m along the x axis. The domain length is chosen such that the MHD patch is large enough to create substantial forces but small enough to minimize the magnet weight.

V. Neptune Entry Case

For the Neptune entry case, the initial geometry and trajectory are taken from Edquist et al. [20]. This geometry is presented in Fig. 5 and provides an L/D = 0.8, trim angle of attack of 40 deg. The freestream velocity is 29.24 km/s with an atmospheric density of 1.45e-4 kg/m^3. Free-stream mass fractions of 0.6246 H_2, 0.2909 He, and 0.0846 CH_4 were assumed. The LAURA simulations were performed with the following species: H_2, H, H^+, He, He^+, e^-, CH_4, CH_3, CH_2, CH, C_2, C, and C^+. The flowfield kinetic rates were taken from a combination of Park [27], Gocken [28], Fujita [29], and Johnston and Brandis [30]. An example of the resulting electron number densities is presented in Fig. 6. Based on these LAURA simulations, the conventional aerodynamic "whole body" value for drag is 565 kN and for lift is 449 kN.

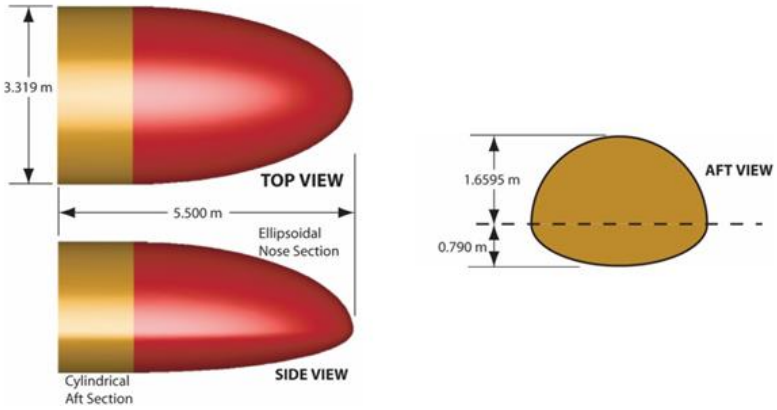

Fig. 5: Geometry definition for the Neptune entry case [20].

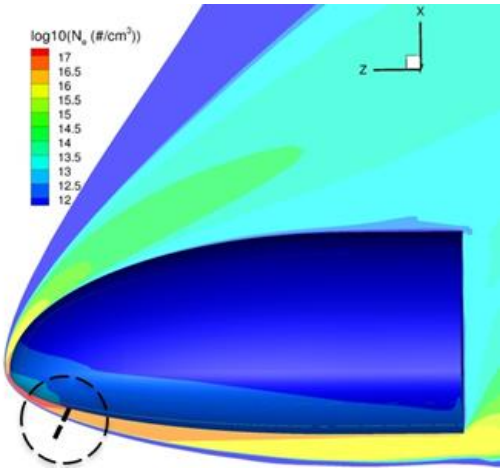

Fig. 6: Electron number densities for the Neptune entry case and the location of the MHD patch identified by the dashed line.

Using the LAURA computed flowfield properties along the body normal line identified in Fig. 6 as inputs, the CFDWARP code was run assuming the configuration defined in Fig. 4. The CFDWARP analysis was performed assuming a total magnetic field strength of 1.0 T, ϕ = 90 deg., and range of magnetic field orientation angles defined by θ. As defined in Fig. 4, the aeroshell surface (bottom face of the volume) is shown in grey. The two electrodes (strips) are shown in red. The dimensions of the MHD patch are 0.2 meters along the x-axis ("bulk" flow direction), 0.118 meters along the y-axis (normal to the aeroshell surface), and 0.1 meters along the z-axis (perpendicular to the "bulk" flow direction). Both electrodes are given the same voltage to represent a short circuit for this initial case. Flow properties are frozen for representing no coupling for this case. Hall effect and ion slip effects are taken into consideration.

The resulting Lorentz forces from the CFDWARP simulations are presented in Fig. 7 as a function of θ. These forces may be converted into lift and drag forces for the Neptune case through the following transformation:

$$L = F_{emfield,x} sin(\alpha + \beta) + F_{emfield,y} cos(\alpha + \beta) \quad (16a)$$

$$D = -F_{emfield,x} cos(\alpha + \beta) + F_{emfield,y} sin(\alpha + \beta) \quad (16b)$$

where α is the angle of attack (40 deg.) and β is the angle of the surface (~10 deg.) from the z-axis in Fig. 6. Figure 7 presents the resulting lift and drag variation as a function of θ. These values are presented in terms of the force per unit area, which allows the results to be scaled to larger MHD patches. Assuming a one square meter patch, the peak drag above 150 kN provides a notable addition to the 565 kN of conventional aerodynamic drag. The lift over most of the θ-space is either negative or a small positive value.

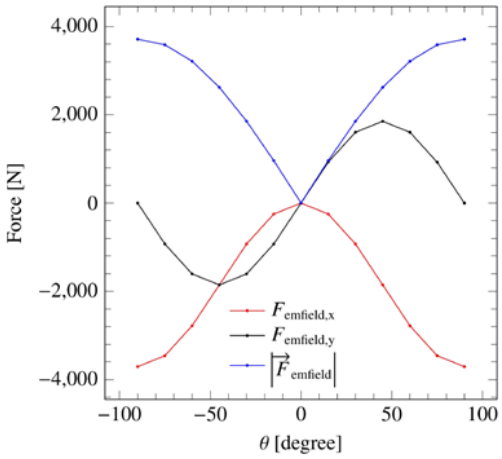

Fig. 7: Lorentz forces for magnetic field orientation angle (θ between -90 and +90 deg.

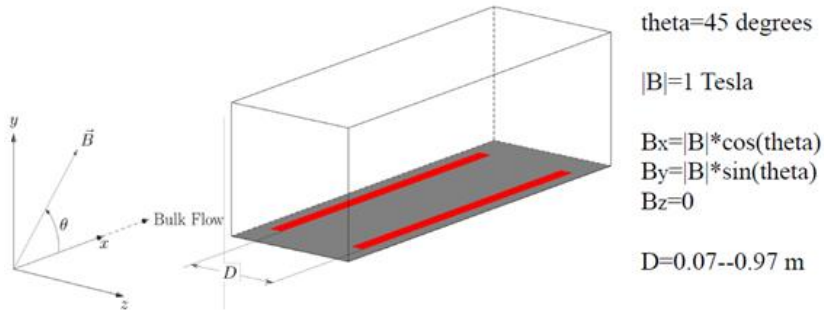

Fig. 8: Computational domain for studying the effects of electrode spacing on the Lorentz forces.

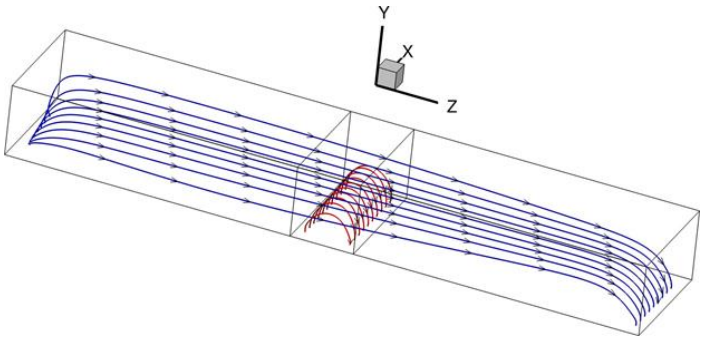

Fig. 9: Effect of distance between electrodes on the current density streamlines; the blue streamlines show the current flowing between the electrodes distanced by 1 m; the red streamlines show the current flowing between the electrodes distanced by 0.1 m.

Additional cases were run to characterize the effects of electrode spacing on the Lorentz forces. Shown in Fig. 8, the volume domain used for this parametric study on electrode spacing is 0.2 meters along the x-axis ("bulk" flow direction) and 0.118 m along the y-axis (normal to the aeroshell surface represented by the grey face on the bottom of

the volume). The dimension in the z-axis (representing the distance between the two electrodes) was varied between 0.1 m to 1.0 m. The 1.0 T magnetic field was locked to θ at 45 deg in the x-y plane and orthogonal to the z-axis.

The effect of distance between electrodes on the current density streamlines is illustrated in Fig. 9. The longer blue streamlines represent the case for D = 0.97 m spacing while the shorter red streamlines represent the case for D = 0.07 m.

The force increases when the distance (D) between electrodes is increased. This effect is due to the current streamlines being more perpendicular to the flow and the magnetic field as D is increased. Indeed, as can be seen from Fig. 9, when the distance between the electrodes is increased, a longer portion of the current streamlines $\vec{J}$, is orthogonal to the magnetic field.

The forces, presented in Fig. 10, reach up to 800 kN/m^2. Hence, a "MHD patch" that encompasses 1 m^2 of the aeroshell can, theoretically, produce up to 800 kN force, which may exceed the total conventional aerodynamic force of 721 kN.

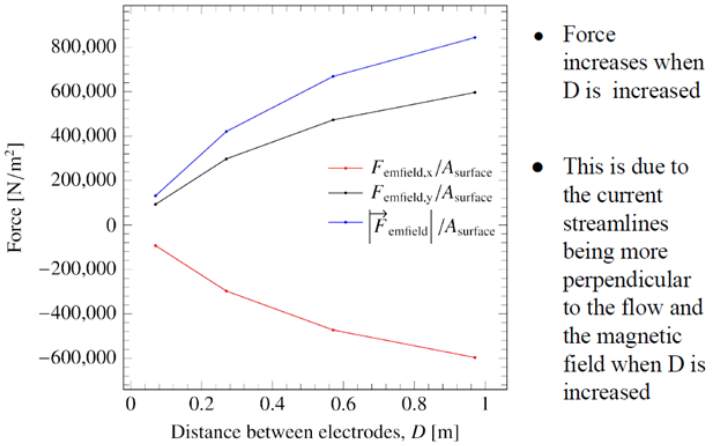

Fig. 10: Effect of electrode spacing on Lorentz forces.

VI. Mars Entry Case

For the Mars entry, a freestream velocity of 9 km/s with an atmospheric density of 4.4x10^{-5} kg/m^3 was modeled for a 70 deg sphere-cone aeroshell at zero deg angle of attack. The entry velocity represents faster transits to Mars. [22-24] The location selected on the 70-deg cone for this case is near the shoulder, as illustrated in Fig. 11. The following species were included in the LAURA simulation: CO_2, N_2, CO, NO, O_2, CN, C_2, C, N, O, N_2^+, CO^+, NO^+, C^+ N^+, O^+, and e-. The chemical kinetics were taken from Johnston and Brandis [30]. The resulting conventional aerodynamic drag from the LAURA simulation is 709 kN, while the lift is zero because of the axisymmetric flow.

Parametric cases were run for understanding the effects of the magnetic field on the conductivity. As explained in Section III above, Hall effects and ion slip effects are generally observed when the atmosphere has very low densities, as in the case of Mars. The dimensions of the volumetric domain selected for this parametric analysis, to represent the initial size of a "MHD Patch" in the location of the aeroshell specified in Fig. 11, are 1.0 m along the x-axis ("bulk" flow direction), 1.0 m along the y-axis (normal to the aeroshell surface), and 1.0 m along the z-axis (perpendicular to the "bulk" flow direction). The magnetic field values between 0.1 T and 3.0 T selected for this parametric case were oriented in the x-y plane at 45 deg, which is orthogonal to the z-axis. Electrode spacing (D) is set to 0.97 m. Both electrodes are given the same voltage to represent a short circuit for this initial case.

The CFDWARP solver calculates the current density streamlines between electrodes for identifying any Hall or ion slip effects. For a magnetic field of 0.1 T, the current density streamlines do not remain parallel, as illustrated in Fig. 12. This current is affected by the Hall effect and flows at an angle of 10-30 deg (from the z-axis), leading to reduced performance of the MHD approach for this Mars case. The performance degrades further as the magnetic field strength is increased. When the magnetic field is increased to 1.0 T, the Hall parameter increases further to a value of 30, leading to severe distortion of the current streamlines shown in Fig. 13 and much reduced performance of the MHD approach, illustrated in Fig. 14.

The impact of the magnetic field strength for the values between 0.1 T to 3.0 T is given in Fig. 14. For comparison, the force calculated using basic MHD equations (nearly vertical dashed line shown in Fig. 14), that do not account for Hall effects and ion slip effect and that also assume the current to flow parallel to the surface, is also shown. The force in the x-direction (in the direction of the "bulk" flow), represented by the red line, illustrates the degradation as the

magnetic field is increased. The slope of the force in the x-direction becomes flatter as the magnetic field strength is increased. The force in the z-axis (in the direction orthogonal to the flow), represented by the black line, increases more or less linearly as magnetic field strength is increased.

In Fig. 14, the ion slip effect reduces the force by a factor of 2, while the Hall effect reduces the force by a factor between 2 and 5. The distance between the electrodes (around 1 meter) is not large compared to the height of the plasma or shock layer thickness (around 0.8 meters). The height of the plasma compared to the distance between electrodes does not constrain the current to flow parallel to the wall for most of the spacing, thus reducing the force by a factor of 5 to 8.

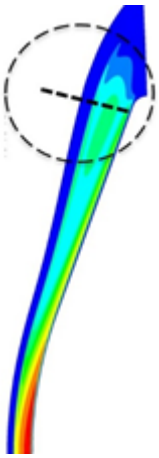

Fig. 11: Electron number densities and MHD patch location for the Mars entry case.

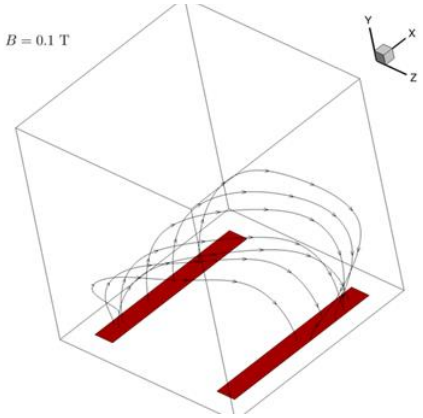

Fig. 12: Current density streamlines between the two electrodes (in red) resulting from B=0.1 T for the Mars entry case.

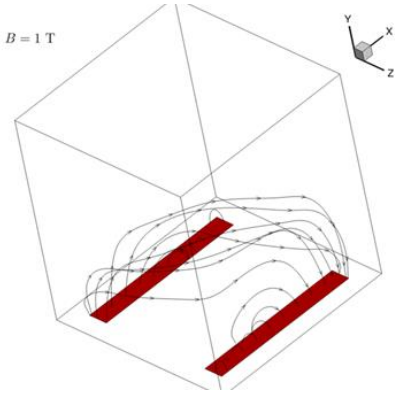

Fig. 13: Current density streamlines between the two electrodes (in red) resulting from B=1.0 T for the Mars entry case.

It should be noted that previous studies on MHD drag and MHD lift for Mars that did not account for the Hall effect, the ion slip effect, or 3D effects have likely overestimated the augmented drag and lift forces. Taking the Hall effect, ion slip effect, and 3D effects into account, Fig. 14 shows that the force magnitudes are on the order of 20 kN for a 1.0 T magnetic field, which is one order of magnitude below the conventional aerodynamic drag value of 709 kN computed by LAURA. However, there may still be some opportunities where this MHD approach could provide suitable levels of augmented drag, augmented lift, and augmented roll. This is an area of future work.

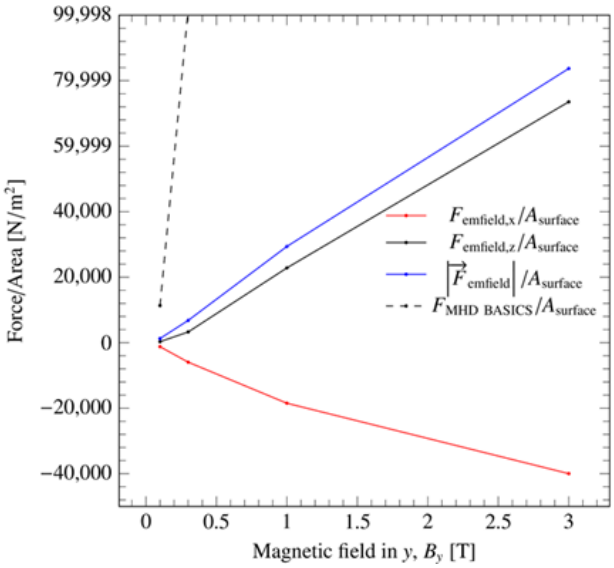

Fig. 14: Impact of magnetic field strength on electromagnetic forces acting on the flow to illustrate Hall and ion slip Effects.

VII. Magnet Mass Estimate

As the electromagnetic flow generated by MHD is conductive, electrical power can be harvested from the flow to power the electromagnet without requiring a separate power supply. The values of current available for extraction in the flow was calculated by CFDWARP for several entry cases and presented in Table 1. These results showed that thousands of amps are available for extraction and use by an electromagnet.

The magnetic system proposed for this MHD approach is based on traditional materials and magnet design guidelines [31]. Five estimates were conducted for 3 different current levels to gain an understanding of their effects on the mass of the electromagnet and heating rate. The first case, shown in Table 1, states the mass (of 370 kg) if a current of 100 amps is used.

Table 1: Coil Mass and Heating Rates Estimates for Several American Wire Gauges (AWG) and Currents

Field Strength (T)	Coil Radius (m)	Wire Gauge (AWG)	Current (amps)	Coil Mass (kg)	Heating Rate (˚C/min)
1	0.56	16	100	370	1725
1	0.56	14	100	585	685
1	0.56	12	100	930	270
1	0.56	12	200	465	1080
1	0.56	12	500	186	6755

By comparison, current lander mission concepts require mass ejection to change the angle of attack. For instance, the Mars Science Laboratory used two 75-kg ballast masses ejected prior to atmospheric entry to force the vehicle to fly at the desired angle of attack. Prior to parachute deployment, six 25-kg ballast weights were ejected prior to drive the angle of attack back to 0 deg nominal. [32] The mass of these 8 ballasts totals 300 kg, roughly the same order of magnitude as the magnet sizes shown in Table 1.

VIII. Future Work

The results of the Phase I Study illustrate that strong Lorentz Forces are present during entries at Neptune and Mars and that the system mass to capitalize on that opportunity to produce additional lift and/or drag is on the order of the ballast mass used for recent lander missions at Mars. However, there are a number of tasks that must be accomplished for maturing this MHD approach for flight demonstration and proof of concept testing. A key aspect of those tasks involves analyzing the amount of time the system is needed to maintain the desired flight path within the prescribed entry corridor and sizing the system accordingly. Illustrated in Fig. 15, the system sizing must consider not only flight mechanics but also thermal loads and heat fluxes. Tasks 1 through 7 were conducted already and some results presented herein. Task 8 is flight mechanics in nature, and POST2 [33] will be used, as explained above. POST2 will also provide an estimate of heating rate and heat flux for calculating thermal loads mentioned in Task 9.

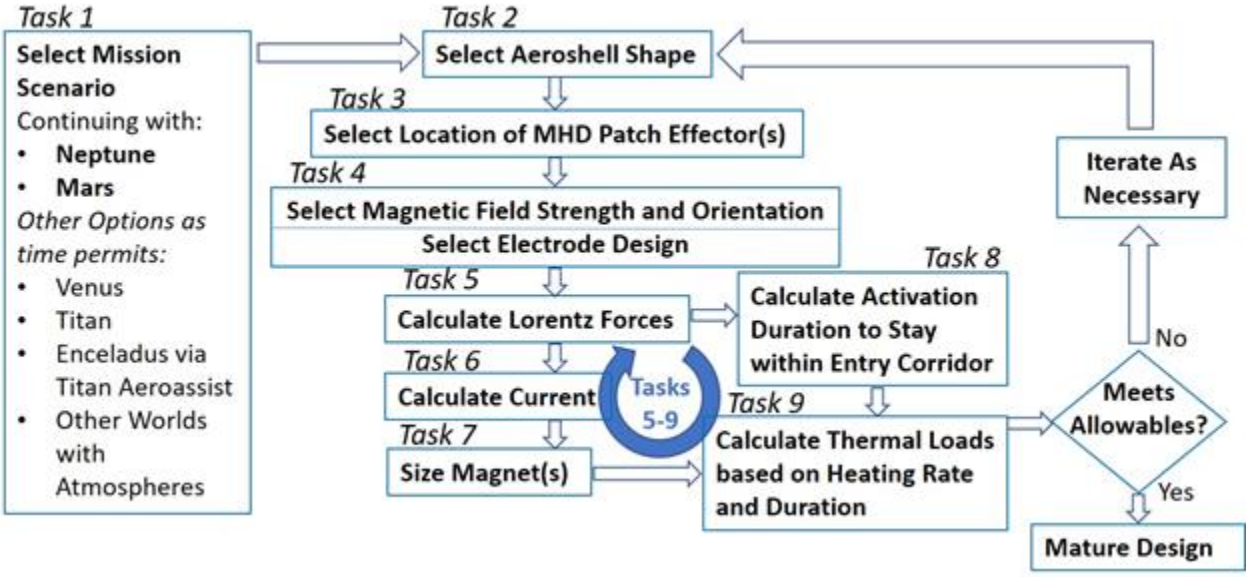

Fig. 15: Proposed Phase II Study Design Process for Addressing Significant Unknowns

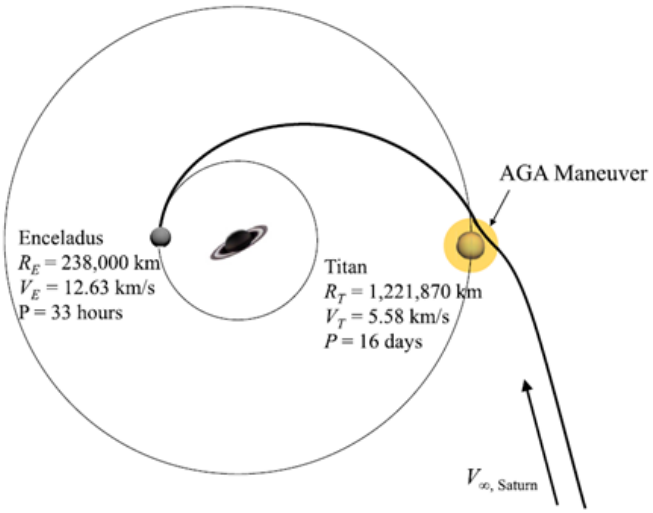

Fig. 16: Orbit diagram showing transfer orbit to Enceladus using Titan aerogravity assist maneuver [34].

Based on the promising Neptune results presented in this work, the performance of this MHD approach will be considered for Titan, Venus, and Earth. Other prior studies for Titan and Venus will provide a benchmark from which to study the MHD approach performance for those two destinations [35, 36]. In general, MHD aerocapture represents a plug-and-play solution for increasing the drag (qC_DA) and L/D of flight-proven, blunt body spacecraft. This unique benefit could enable complex mission architectures to high-priority destinations without incurring the substantial

development time and cost of a new flight vehicle. Future work will examine the ability of this technology to deliver a flagship class satellite into orbit around Enceladus, highlighted in Fig. 16. The mission will utilize an aerogravity assist maneuver in Titan's atmosphere [34, 37] to deliver the probe into an elliptical orbit about Saturn with apogee and perigee at Enceladus and Titan, respectively. Enceladus orbit insertion is achieved with a relatively modest delta-v (~650 m/s) following a series of moon-tour maneuvers. The use of MHD aerocapture will substantially reduce the heating rate and total heat load at Titan, increase the entry corridor width, and enable precise delivery of the spacecraft into the Enceladus transfer orbit, thus minimizing the propellant mass required for post-transfer orbit corrections.

IX. Conclusion

The MHD approach creates lift and drag equaling the aerodynamic forces for the entry cases presented for Neptune and Mars. In some cases, the resulting L/D ratio exceeded 1.0. For the case of Mars, where Hall and Ion slip effects dominate the flow due to the low atmospheric density, rolling moments can be produced as well as lift and drag forces. Additional work is envisioned for demonstrating this new aerocapture approach.

As the results of this study illustrate that MHD can generate large steering forces, this approach potentially allows entirely new spacecraft shapes to be considered for Neptune as well as smaller decelerators to be analyzed for Mars. For instance, a blunt body aeroshell equipped with this MHD approach may satisfy the stringent L/D ratio necessary for maintaining control of the spacecraft during the tight entry corridor at Neptune. Considering the promising results for Neptune and Mars, this MHD approach offers potential application at Titan [35], Venus [36] and at Earth and forms the basis for proceeding with a Phase 2 design study on how best to implement this MHD approach into a variety of human destinations and science missions.

This MHD approach may enable new missions that recent scenario studies indicate a huge benefit from an aerodynamic assist maneuver such as Titan aerogravity assist to deliver a Flagship class satellite into orbit around Enceladus.[34, 37] Analysis for these destinations could be included in a follow-on study. The analysis results, if verified via flight demonstration testing (similitude at Earth), could revolutionize Entry, Descent, and Landing (EDL) at other worlds with atmospheres and significantly modify mission architecture not only for those worlds but also for Return to Earth from the Moon and Mars.

Acknowledgments

The authors thank NASA Innovative Concepts (NIAC) for the support and funding that made this study possible.

References

[1] Moses, Robert W., Cheatwood, F. McNeil, Johnston, Christopher O., Green, Justin S., Williams, R. Anthony, Macheret, Sergey O., Parent, Bernard, Little, Justin, Austin, Matthew, Aldrin, Andrew, "Advanced Aerocapture System for Enabling Faster-Larger Planetary Science & Human Exploration Missions," (19-NIAC20B-0128), Final Phase I Report: NASA Innovative Advanced Concepts (NIAC), FY 20 NIAC Phase I Solicitation, (80HQTR19NOA01-20NIAC-A1), February 26, 2021.

[2] Moses, R., "Regenerative Aerobraking," Paper-057, Space Technology and Applications International Forum (STAIF-2005); 13-17 Feb. 2005; Albuquerque, NM; United States.

[3] Moses, R.W., Kuhl, C.A., Templeton, J.D., "Plasma Assisted ISRU at Mars," 15th International Conference on MHD Energy Conversion; 24-27 May 2005; Moscow; Russia

[4] Steeves, C., Shneider, M.N., Macheret, S.O., Miles, R.B., Wadley, H., and Evans, A., "Electrode Design for Magnetohydrodynamic Power Panels on Re-Entering Space Vehicles," Paper AIAA-2005-1340, 43rd AIAA Aerospace Sciences Meeting and Exhibit, Reno, Nevada, Jan. 10-13, 2005.

[5] Macheret, S.O., Shneider, M.N., Candler, G.V., Moses, R.W., and Kline, J.F., "Magnetohydrodynamic Power Generation For Planetary Entry Vehicles," AIAA 2004-2560, 35th AIAA Plasmadynamics and Lasers Conference, 28 June – 1 July 2004, Portland, Oregon.

[6] Vuskovic, L., Popovic, S., Drake, J., and Moses, R., "Magnetohydrodynamic Power Generation in the Laboratory Simulated Martian Entry Plasma," 15th International Conference on MHD Energy Conversion; 24-27 May 2005; Moscow; Russia.

[7] Wan, T., Candler, G.V., Macheret, S.O., and Shneider, M.N., "Three-Dimensional Simulation of the Electric Field and Magnetohydrodynamic Power Generation During Reentry," AIAA Journal, Vol. 47, No. 6, 2009, pp. 1327-1336

[8] Ali, H. and Braun, R., "Effects of Magnetohydrodynamic Energy Generation on Planetary Entry Vehicle Flight Dynamics", 13th International Energy Conversion Engineering Conference, AIAA Propulsion and Energy Forum, (AIAA 2015-4179), July 27-29, 2015, Orlando, FL.

[9] Kim, M. and Boyd, I., "Effectiveness of a Magnetohydrodynamics System for Mars Entry," Journal of Spacecraft and Rockets, Vol. 49, No. 6, November-December 2012, pp. 1141-1149.

[10] Smith, D., Gildfind, D., James, C., McIntyre, T., and Wheatley, V., "Magnetohydrodynamic Drag Force Measurements in an Expansion Tube," AIAA-2018-3755, AIAA Aviation Forum, 2018 Flow Control Conference, June 25-29, 2018, Atlanta, GA.

[11] Fujino, T., Yoshino, and Ishikawa, M., "Numerical Analysis of Reentry Trajectory Coupled with Magnetohydrodynamics Flow Control," Journal of Spacecraft and Rockets, Vol. 45, No. 5, September-October 2008, pp. 911-920.

[12] Gildfind, D., Smith, D., Lewis, S., Kelly R., James, C. Wei, H., and McIntyre, T., "Expansion Tube Magnetohydrodynamic Experiments with Argon Test Gas," AIAA-2018-3754, AIAA Aviation Forum, 2018 Flow Control Conference, June 25-29, 2018, Atlanta, GA.

[13] Kawamura, M., Nagata, Y., Katsurayama, H., Otsu, H., Yamada, K., and Abe, T., "Magnetoaerodynamic Force on a Magnetized Body in a Partially Ionized Flow," Journal of Spacecraft and Rockets, Vol. 50, No. 2, March-April 2013.

[14] Ali, H., “Magnetohydrodynamic Energy Generation and Flow Control for Planetary Entry Vehicles,” Doctoral Dissertation, Daniel Guggenheim School of Aerospace Engineering, August 2019.
[15] Kenjeres, S. and Hanjalic, K. ‘‘On the implementation of effects of Lorentz force in turbulence closure models,’’ Int. J. Heat Fluid Flow, Vol. 21, p. 329, 2000.
[16] Gülhan, A., Esser, B., Koch, U., Siebe, F., Riehmer, J., Giordano, D., and Konigorski, D., “Experimental Verification of Heat-Flux Mitigation by Electromagnetic Fields in Partially-Ionized-Argon Flows,” Journal of Spacecraft and Rockets, vol. 46, 2009, pp. 274–283
[17] Thompson, K., Hollis, B., Johnston, C., Kleb, B., and Lessard, V., “LAURA Users Manual: 5.6,” NASA TM 2020-220566, 2020.
[18] Parent, B., Shneider, M. N., and Macheret, S. O., “Detailed Modeling of Plasmas for Computational Aerodynamics,” AIAA Journal, Vol. 54, No. 3, 2016, pp. 898–911.
[19] Lockwood, Mary Kae, “Aerocapture Systems Analysis for a Neptune Mission,” AIAA 2004-4951, AIAA Atmospheric Flight Mechanics Conference and Exhibit, 16-19 August 2004, Providence, Rhode Island
[20] Edquist, Karl T., Prabhu, Ramadas K., Hoffman, David A., and Rea, Jeremy R., “Configuration, Aerodynamics, and Stability Analysis for a Neptune Aerocapture Orbiter,” AIAA 2004-4953, AIAA Atmospheric Flight Mechanics Conference and Exhibit, 16-19 August 2004, Providence, Rhode Island
[21] Hughes, S., Cheatwood, F., Calomino, A., Wright, H., Wusk, M., and Hughes, M., “Hypersonic Inflatable Aerodynamic Decelerator (HIAD) Technology Development Overview,” AIAA 2011-2524, 21st AIAA Aerodynamic Decelerator Systems Technology Conference and Seminar, 23-26 May 2011, Dublin, Ireland.
[22] Komar, David R. and Moses, Robert W., "Hercules Single-Stage Reusable Vehicle supporting a Safe, Affordable, and Sustainable Human Lunar & Mars Campaign", AIAA SPACE and Astronautics Forum and Exposition, AIAA SPACE Forum, (AIAA 2017-5288), AIAA SPACE 2017 Conference; 12-14 September 2017; Orlando, FL; United States
[23] Machado, Larissa Balestrero, Wilde, Markus, Kaplinger, Brian, and Moses, Robert, “Mars Aerocapture and Subsystems Analysis for a Cycler Orbit Crew Transfer Vehicle,” 2018 AAS/AIAA Astrodynamics Specialist Conference, 19-23 August 2018, Snowbird, UT, United States
[24] Moses, Robert W., Bushnell, Dennis, Komar, David R., Singleterry, Robert C., Choi, Sang, Litchford, Ronald, Chang-Diaz, Franklin, and Carter, Mark, "Maintaining Human Health for Humans-Mars", 2018 AIAA SPACE and Astronautics Forum and Exposition, AIAA SPACE Forum, (AIAA 2018-5360), 17-19 September 2018, Orlando, FL, United States
[25] Thompson, Kyle B., Johnston, Christopher O., Hollis, Brian R., and Victor Lessard, “Recent Improvements to the LAURA and HARA Codes,” AIAA 2020-3030, AIAA Aviation 2020 Forum, June 15-19, 2020, Virtual Event.
[26] B Parent, MN Shneider, SO Macheret. “Generalized Ohm's law and potential equation in computational weakly-ionized plasmadynamics”, Journal of Computational Physics, Vol. 230 (4), Pages 1439-1453, 2011.
[27] Park, C. “Nonequilibrium Ionization and Radiation in Hydrogen Helium Mixtures”, Journal of Thermophysics and Heat Transfer, Vol. 26, No. 2, 2012, pp. 231 - 243.
[28] Gocken, T., “N2-CH4-Ar Chemical Kinetic Model for Simulations of Atmospheric Entry to Titan,” Journal of Thermophysics and Heat Transfer, Vol. 21, No. 1, 2007, pp. 9 - 1.
[29] Fujita K, Yamada T, and Ishii N., “Impact of Ablation Gas Kinetics on Hyperbolic Entry Radiative Heating,” AIAA Paper 2006-1185, 2006.
[30] Johnston, C. O., and Brandis, A. M., “Modeling of Nonequilibrium CO Fourth-Positive and CN Violet Emission in CO2-N2 Gases, Journal of Quantitative Spectroscopy and Radiative Transfer, Vol. 149, 2014, pp. 303 - 317.
[31] Kelly, Charles L. and Little, Justin M., “Performance Scaling and Mission Applications of Drag-Modulated Plasma Aerocapture,” IEPC-2019-202, Presented at the 36th International Electric Propulsion Conference, University of Vienna, Austria, September 15-20, 2019
[32] https://en.wikipedia.org/wiki/Mars_Science_Laboratory
[33] “Program to Optimize Simulated Trajectories II (POST2)”, NASA, https://post2.larc.nasa.gov/
[34] Lu, Ye, and Sarag J. Saikia. "Titan aerogravity-assist maneuvers for Saturn/Enceladus missions." Acta Astronautica (2020).
[35] Lockwood, Mary K., Queen, Eric, Way, David W., Powell, Richard W., Edquist, Karl, Starr, Brett W., Hollis, Brian R., Zoby, E. Vincent, and Glenn A. Hrinda, Robert W. Bailey, Jeffery L. Hall, Thomas R. Spilker, Muriel Noca, Robert Haw, Carl G. Justus, Aleta Duvall, Dale L. Johnson, James Masciarelli, Naruhisa Takashima, Kenneth Sutton, Joe Olejniczak, Bernard Laub, Michael J. Wright and Dinesh Prabhu, R. Eric Dyke, “Aerocapture Systems Analysis for a Titan Mission,” NASA/TM-2006-214273, February, 2006
[36] Girija, Yu, and Saikia, “Feasibility of Mass-Benefit Analysis of Aerocapture for Missions to Venus,” Journal of Spacecraft and Rockets, 57(2): 1-16, January 2020
[37] Ramsey, Philip, and James Evans Lyne. "Enceladus Mission Architecture Using Titan Aerogravity Assist for Orbital Capture About Saturn." Journal of Spacecraft and Rockets 45.3 (2008): 635-638.